A study on the effects of forced air-cooling enhancements on a 150 W solar photovoltaic thermal collector for green cities

Anurag Shrivastava [a,*], J. Prakash Arul Jose [b], Yogini Dilip Borole [c], R. Saravanakumar [d], Mohsen Sharifpur [e,f,*], Hossein Harasi [g,*], R.K. Abdul Razak [h], Asif Afzal [h,i,*]

[a] *Lakshmi Narain College of Technology and Science, Indore, India*
[b] *Department of Civil Engineering, Paavai Engineering College, Namakkal, India*
[c] *Department of Electronics and Telecommunications Engineering, G.H. Raisoni Institute of Engineering and Technology, Pune, Maharashtra, India*
[d] *Department of. Wireless Communication, Institute of ECE, Saveetha School of Engineering, Saveetha Institute of Medical and Technical Sciences, Chennai, India*
[e] *Clean Energy Research Group, Department of Mechanical and Aeronautical Engineering, University of Pretoria, Pretoria 0002, South Africa*
[f] *Department of Medical Research, China Medical University Hospital, China Medical University, Taichung 404, Taiwan*
[g] *Young Researchers Club, Ardabil Branch, Islamic Azad University, Ardabil, Iran*
[h] *Department of Mechanical Engineering, P. A. College of Engineering (Affiliated to Visvesvaraya Technological University, Belagavi), Mangaluru 574153, India*
[i] *Department of Mechanical Engineering, School of Technology, Glocal University, Delhi-Yamunotri Marg, SH-57, Mirzapur Pole, Saharanpur District, Uttar Pradesh, 247121, India*

A R T I C L E I N F O

Keywords:
Solar photovoltaic thermal collector
Solar radiation
Baffles
Fins
Computational fluid dynamics

A B S T R A C T

The major goal of this research is to identify optimal arrangement of forced cooling enhancements such as baffles and fins. This research focuses to determine the effect of the different configurations for achieving higher thermal efficiency of the 150 W solar photovoltaic thermal collectors (PV/T). The air-cooling enhancements evaluated in this PV/T system are free duct without fins, ducts with fully transverse fins, partially transverse fins, longitudinal fins with straight baffles and inclined baffles. The experiments are done on hot days of summer in May 2018, India and achieved diverse flow rates of air mass ranging from 0.012 to 0.016 kg/s. The Reynolds number obtained in the flow experiments are in the range of 900–1300 and Nusselt number 35–130.A Computational fluid dynamics study was established to achieve a parametric research to determine surface and outside profiles to study the cooling effectiveness. The impacts on flow rate of air mass on the outlet T, Reynolds Number, coefficient of heat transfer and Nusselt number were studied. The maximum irreversibility occurred at the free type fins whereas minimum irreversibility obtained at longitudinal type with inclined baffles and detected that PV/T system have a prodigious impact on the energy efficacy as well as energy losses increased with increasing surface T. This research displayed that the coefficient of heat transfer of solar panel upsurges by means of growing Reynolds number. Additionally, the PV module thermal efficacy by growing flow rate and reduced with increasing friction factor. An increase by 6–8% in exergy efficiency and 5% to 7% in energy efficiency was recorded while using these forced air-cooling enhancements. A reasonable agreement was reached between experimental and computational model. The exergy performance was increased from 20% to 28 % while using air cooling duct with longitudinal fins and inclined baffles. The thermal energy performance was increased from 12 to 18 % while using air cooling duct with longitudinal fins and inclined baffles. This is the maximum energy efficiency achieved in this PV/T system with the Nusselt number ranging from 30 to 130 and Reynolds number 900–1300. This study showed that Nusselt number of PV/T system upsurges with growing Reynolds number of air flow. The PV module thermal efficacy upsurges by means of growing flow rate as the friction factor increases. The longitudinal fins with inclined baffles provided higher friction factor, thereby ensured higher heat transfer rate. The fins and baffles employed in our research are economical and relaxed to manufacture and install. They bid a fairly lower friction lack in movement of air and henceforth do not necessitate higher fan power. This set up can be used for green and smart cities as it helped to reduce the energy consumption considerably.

* Corresponding authors at: Department of Medical Research, China Medical University Hospital, China Medical University, Taichung 404, Taiwan (M. Sharifpur). Department of Mechanical Engineering, P. A. College of Engineering (Affiliated to Visvesvaraya Technological University, Belagavi), Mangaluru 574153, India (A. Afzal).

E-mail addresses: anuragshri76@gmail.com (A. Shrivastava), mohsen.sharifpur@up.ac.za (M. Sharifpur), hossein_harasii@yahoo.com (H. Harasi), asif.afzal86@gmail.com (A. Afzal).

Nomenclature

C_p	Specific heat of air, J/kg k
D_h	Hydraulic diameter passage, mm
f_f	Friction factor, dimensionless
H_D	Height of duct, mm
h_c	Convective heat transfer coefficient, W/m^2 K
K	Thermal conductivity, W/m K
L_P	Length of passage, mm
Nu	Nusselt number, dimensionless
$\dot{m}$	Mass flow rate of air, kg/s
Pr	Prandtl number, dimensionless
$(\Delta p)_0$	Pressure drop across the orifice plate, Pa
Q_h	Useful heat gain, W
Re	Reynolda number, dimensionless
T_{ain}	Temperatures of inlet air, K
T_{a0ut}	Temperatures of outlet air, K
T_{film}	Mean air temperature, K
V_a	Velocity of air, m/s
W_P	Width of passage, mm
q	Heat Transfer
TP	Thermal performance
STC	Solar thermal collector

Greek Letters

μ	Absolute velocity of air, m^2/s
ρ	Density of air, kg/m^3
ν	Kinematic viscosity of air, m^2/s

Introduction

Many old cities are being transformed to green and smart cities these days. Older cities can benefit enormously from being greened. Green and smart are complementary and would provide practical and intangible advantages. It has been discovered that by increasing the use of solar thermal, solar photovoltaic, and wind energy, current cities may achieve a 10–12 percent reduction in power demand [1,2].A solar PV/T system, often known as a PV/T collector, transforms solar energy into both electrical and thermal energy. It's a system that converts sunlight into electricity power with a solar thermal collector that captures the remaining energy while also removing heat from a photovoltaic (PV) module. Because of this configuration, PV/T has a greater total energy efficiency than solar PV and a separate solar thermal collector. In most cases, an increase in T owing to heat generation affects the efficiency of PV cells while they are in operation. As a result, a heat transporting mechanism in PV cells is required to provide a cooling impact on the cells while also lowering the resistance, resulting in an increase in efficacy [3,4]. A PV/T air collector is essentially a hollow conductive metal framework for mounting PV panels. These panels transfer heat into the covered space of a shallow metal box, where air is circulated. Conductive energy loss was caused by T changes between the PV module and other substances with which the PV module came into contact. A PV module's heat resistance determined its ability to transport heat to its surroundings [5-8].

The main advantage of using PVT, apart from lowering the operational temperature of photovoltaic cells, is combining two installations that have worked separately till now into one. So less space is required for the installation. A disadvantage of the system is the interdependence of the two systems. The most appropriate time for the operation is the summer period which is characterized by high insulation and high temperatures. Another disadvantage of PVT is the scale of the system. In the case of installations fitted on detached house, the photovoltaic system often takes the area of over a dozen to several dozen m^2, which means that a problem with consuming such a large amount of heat can arise in the summer period. At the same time, a hybrid PV/T will generate considerably higher heat loss than a standard collector installation in the winter period due to the lack of a selective absorber and the appropriate thermal insulation.

In PV modules, heat transfer (HT) which is convective occurred among blowing air and the hot surface of module. As the air has low heat transfer coefficient, the thermal efficacy of PV/T system originating was small. Improvement in heat transfer coefficient can be achieved through as long as artificial unevenness by an increment of pressure drop. Therefore, there was an essential requirement to enhance the system constraints to exploit heat transfer, by possession the friction losses minimal [9-12].

The effectiveness and thermal modelling of a dual channel quasi PV/T module was studied by Singh et al. [2]. Bombarda et al. [3] applied the first and second laws of effectiveness for equivalence of a roll-bond arrangement with typical tube and sheet. Hedayatizadeh et al. [4] studied the energy loss of air heater (solar) with v-corrugated plate which is double-pass/glazed. Bahrehmand along with Ameri [5] determined the energy and effectiveness of solar air collector with a single and two cover glasses using mathematical model. When comparing corroded solar air heaters to smoother flat-based plate solar air heaters, Yadav and Kaushal [6] found that roughened solar air heaters had a higher exergetic efficiency.

Singh et al. [7] offered the affectedly rib coarsened solar air heaters by the conventional flat-plate heater. Ozgen et al. [8] explored double channel solar air heater (flat-plate) empirically, designing along with testing multiple types of absorber plates in varying air flow rates. Lalji et al. [9] did an analytical study and provided the friction statistics and HT for solar air heater (packed-bed) in varied rates of mass flow. Agarwal and Tiwari [10] evaluated energy efficiency of glossy hybrid PV/T module collectors towards PV modules. Teo et al. [11] found that whenever an improvement in air mass flow rate, electrical and thermal efficiencies also get.

At midday, Bambrook and Sproul [12] investigated solar PV/T system in Sydney, finding higher efficiency of 28–55 percent and PV efficiency of 10.6 percent to 12.2 percent. Alta et al. [13], Esen [14], Akpinar and Koçyiit [15], and Moummi et al. [16] demonstrated type of air heaters (solar) with fins or without fins and assessed energy analyses by varied flow rate. Chen et al. [17] projected a PV/T system using triple junction solar cells and used experiments and simulation to determine the thermal efficiency. Missirlis et al. [18] looked into the influence of different polymer solar collector designs on heat transfer. Agarwal and Tiwari [19] inspected the energy as well as energy gain of diverse kinds of PV heat air collector for the environment of Srinagar, India. They came to the conclusion that a glazed collector had a higher energy yield than an unglazed one.

Sabzpooshani et al. [20] examined the theoretical impacts of various geometrical shapes on the baffle type solar water heater. In moderate mass flow rate, he found that fins and baffles dramatically improved energy efficiency. Mohammadi and Sabzpooshani [21] introduced 3 baffled solar air heaters of 3 types and performed an energy saving study, finding that the both fins and baffles improved system efficiency. The double-pass solar collector without fins and with fins was achieved by Fudholi et al. [22]. Bahrehmand and Ameri [5] developed a scientific model for glass collectors, as well as the energy efficacy of two kinds of collectors. Under real-world settings, Bombarda et al. [3] perform a statistical research on roll-bond configurations by traditional sheet and tube and three kinds of PVT modules. Hedayatizadeh et al. [23] investigated energy loss of a glazed/ double-pass v-corrugated plate solar air heater and developed a thermal study. Singh et al. [2] evaluate effectiveness and thermal simulation in double channel semi-transparent

PVT modules, as well as other PVT system configurations. Ross et al. [24] used CFD methods to analyse the PV system's module T and stress outcomes, as well as the electrical output. The combination PV/solar thermal façade was tested by Smyth et al. [25] and contrasted incorporated flat collector. Also did research on electricity generation, collector efficiency, and unglazed and double-glazed hybrid PV/solar thermal façades. The PV panel thermal characteristics with its phase change material were investigated by Sourav et al. [26]. They also looked at wind direction, wind velocity, phase change material melting T, and ambient T under different operational settings.

Mohammad Hossein, et al. [27] investigated the efficacy of a solar tower with a Rankine cycle using the 1st and 2nd laws of thermodynamics. A numerical technique has been used in the GNU Octave environment to compute the appropriate value of energy and exergy losses in each element. They found that the central receiver system suffers the most exergy loss, whereas the turbine in the power block suffers the greatest energy loss. A numerical analysis of a solar heat exchanger with baffles was performed by Younes et al. [28]. As a working fluid, H_2 gas was used. The impact of various channel obstructions was investigated. They demonstrated that their proposed design of a solar heat exchanger filled with H_2 gas improves overall thermal performance significantly and may be employed in a range of thermal equipment. Benaissa, et al. [29] proposed a new approach for increasing greenhouse still productivity and extending solar distillation overnight. Thermal energy was generated using a concentrator, a greenhouse still, whereas the photovoltaic solar energy was generated utilising panels in this system. In comparison to previous distillers, they found that the proposed technology was extremely productive. Lavinia et al. [30] used two different solar thermal collector designs to accomplish exergy-based optimization. They employed a collection of control sensors to manage the system's performance and monitor design factors such as the fluid's intake and outlet temperatures, air temperature, received solar flux, and necessary mechanical and electrical effort. They found that according to the Exergy analysis, further temperature control is required for optimization. Ravindra et al. [31] offered a design proposal for a revolutionary biomass gasifier. The system allows both for solar capture and gasification. A heat pipe system transports heat from the solar receiver to the gasifier. By reducing the focal height of the cavity receiver, they were able to increase the average solar flux. Mohamad, et al. [32] examined the efficacy of a LiBr-H_2O absorption refrigeration system and found that it may be improved by employing solar energy and Nano fluids. Prior to passing to the generator, the fluid was warmed in a trough collector. They used four different types of Nano fluids for their study. When compared to pure water, they observed that employing Ag nanoparticles at a concentration of 2.4 percent enhances the COP by 3.8 percent. Younes et al. [33] increased a duct's thermal performance by changing and reconstructing its interior geometry. Novel 'V' shape fins with varying dimensions have been presented and are arranged in a periodic pattern across the duct walls. The analysis revealed that a 40-degree attack angle with a factor of thermal enhancement of 2.2 was the best case for the maximum value of Reynolds number. Furthermore, Younes, et al. [34] investigated dynamic field simulations of a horizontal duct with three obstacles and oil as the working fluid. The proposed new forms of oil-filled heat exchangers, which include case (A) with 1 fin and 2 baffles and case (B) with 2 fins and 1 baffle, enhance the dynamic thermal energy behaviour of a variety of thermal devices, including solar collectors. Milad, et al. [35] used Artificial Neural Network k to assess the thermal efficacy of a flat-plate collector.

Mohsen et al. [36] found that solar energy can be applied in desalination systems in order to provide required heat or generate needed electricity by using PV modules. Applying solar energy instead of fossil fuels leads to more environmentally benign technologies in desalinating saline water. Due to the severe worldwide water crisis, precise comprehension of desalination methods can pave the way toward potable water achievement at reasonable cost. Lower greenhouse gases emission and high operation reliability are their advantages. Maleki et al. [37] studied Phase Change Materials (PCMs) in different solar energy systems for thermal energy storage and performance enhancement. Improving heat transfer from PCMs leads to reductions in charge and discharge durations, which makes them more favourable as storage units. The studies in this field reveal that employing nanotechnology is an efficient method for heat transfer improvement. The improvement in thermal performance due to nano PCMs increased thermal conductivity and decreased latent heat of fusion.

Zhang et al. [38] presented a unique aluminium–graphite dual-ion battery (AGDIB) having excellent reversibility and energy density. Tong et al. [39] satisfactorily developed a unique pAl/C-G DIB that showed excellent rate capability with reversible capacity. A unique potassium-ion-based dual-ion battery system based on a potassium-ion electrolyte, was developed by Bifa et al [40], integrating benefits of both the batteries. Wang et al. [41] presented a Calcium-ion batteries that can function reliably at ambient temperature in a novel cell structure using graphite as the cathode and tin foils as the anode. To produce tin pyrophosphate Nano dots, Sainan et al. [42] presented a molecular grafting approach. This system had a great specific capacity, good rate capability and cycle stability. A solar collector corrugated with ribs was examined by Raj Kumar et al [43] for thermal increase. They found that the jet impingement and roughness play a significant role in enhancements of heat transfer among the different approaches utilised to improve STC performance. Santhosh Kumar et al. [44], experimentally investigated traditional solar panel with different duct arrangements for three days in four different modes for heat removal. Because of the higher evaporation speed and lower photovoltaic panel temperature, the suggested method considerably improved photovoltaic panel performance. The experimental study of a solar air heater with double pass (SAHD) arrangement on the absorber surface with various porous materials by Raj Kumar et al. [45]. Aluminium was determined to have the most effect on the effectiveness of SAHD out from the three materials employed in the experiment.

Despite these, there are significant contributions made by researchers towards the air cooling enhancements for PV/T systems, still the exergy losses are recorded at higher rate. In turn, the optimized design of forced air-cooling enhancement structures is essentially required to increase the heat transfer rate. However, no much references are available in the literature on fins and baffles arrangement for reducing the T rise of PV/T systems. To address this research gap, this study is planned to evaluate the different designs of fins and baffles arrangement to upsurge the heat removal rate. The objective of this experimental and computational research is to (a) analyse the impact of five forced air-cooling arrangement of enhancements such as free duct, duct with fully transverse fins, duct with partially transverse fins, duct with longitudinal fins and straight baffles and duct with longitudinal fins and inclined baffles on energy efficacy along with energy of a 150 W solar PV/T collector. (b) Develop a Computational fluid dynamics (CFD) study for conducting a parametric study on PV/T system for diverse air mass flow rates to analyse the cooling effectiveness of enhancements.

Experimental set up

The experimental arrangement was intended, invented and confirmed in Ashoka College of Engineering, Hyderabad. Researches were accepted out from April to June 2019 at Chennai, India (13°06 ´North and 80°18´East, tropical climate). Readings were recorded between 9 am and 4 pm in all days of physical experiments. Energy analysis was performed by means of the first law of efficiency. First law efficiencies relate to the conversion of energy from one form to another and conservation of the overall quantity of energy, without direct consideration for the quality of energy. The exergy study was conducted to find energy fatalities during the PV conversion method through using the second law of efficiency.

The photovoltaic thermal system (PV/T) comprises of three main parts such as (1) PV thermal unit (2) air blower with pipe arrangement

(3) data logger. The layout and photographic view of experimental set up of PV/T system by means of air cooling enhancements are given in the Figs. 1(a) and (b).The specification of PV/T system, details of air-cooling enhancements and operating constraints are stated in Tables 1, 2 and 3 respectively. The PV/T system consisted of transparent cover, absorber plate, insulation substance, frame, air passage channel with fin and baffles. The thickness of the plywood is 15 mm and the material is coated in dark blue colour. The size of air pathway is 1470 X 645 X 80 mm that was wrapped entirely to evade warm air seepage. The angle of the solar PV/T system has been static at 13° according to Chennai meteorological site. The PV/T system was placed in such a way that no shadows fall on the system and at a distance of 120 mm from the pounded to avert rainfall and any normal sources. The PV/T system was straddling on a galvanized metal frame wherein light energy or solar energy fleeting over the glazing surface. The condition of PV/T scheme is listed in the Table 1.

The air-cooling enhancements tested in this set up are free duct, ducts with fully transverse fins, partially transverse fins, longitudinal fins with straight baffles and longitudinal fins with inclined baffles as shown in the Fig. 2(a) through Fig. 2(e). The details of air cooling enhancements are shown in the Table 2.

The air properties and operating parameters used for testing are given in Tables 3 and 4.

Uncertainty analysis

To avoid errors, all of the devices were calibrated prior taking test readings. Voltmeter, T sensor, anemometer, pyranometer, ammeter, and pressure gauges were all part of the PV/T setup. The mercury thermometer was used to limit the ambient air T. Thermocouples are used to control the inlet, outside air T, glazing surface T, and tedlar T. Thermocouples are put in the right location of the PV/T system. The air flow was adjusted using a valve between the blower and the air channel's entrance. The solar rays were stifled by a pyranometer, which was placed near the collection surface.

The delivered air and wind velocities were controlled using a cup anemometer and a Lutron AM-4206 M digital anemometer, respectively. The current and voltage were regulated using a data logger's standardised ammeter and voltmeter. Each piece of data was collected at 15-minute intervals and stored in a data logger. Table 5 lists the uncertainties that occurred throughout the measurement.

Analysis methodology

Energy study of PV/T

The electrical efficacy of a PV system is described as a proportion of actual electrical yield power and input amount of incident solar energy above PV surface, are given below [46,47]:

$$\text{Electrical efficacy , } \hat{I}_{\cdot e} = \frac{V_p I_p}{S} = \frac{E_e}{S} \tag{1}$$

Where E_e is electrical power and solar absorbed flux (S)

Mass flow rate of air can be found as

$$Density, \rho = \frac{P}{R\,T_{air}} \tag{2}$$

Where P is the pressure in N/m^2, T_{air} is the air temperature in K, R is the universal gas constant (J/kg/K)

$$Mass\ flow\ rate\ \dot{m} = \rho A_m v \tag{3}$$

The thermal efficacy of a PV/T was demarcated as the proportion among increase of energy and the solar radiation incident on the collector surface

$$Q = \dot{m}\, C_p (T_{out} - T_{in}) \tag{4}$$

$$\eta_t = \frac{\dot{m}\, C_p (T_{out} - T_{in})}{A_m G} \tag{5}$$

Where Q, G, $\dot{m}$,C_p, A_m and η_t are the rate of useful thermal energy, solar radiation intensity, the mass flow rate of flowing air, the heat capacity of flowing air, the area of air duct, and PV/T air collector thermal efficiency, respectively

Exergy study of PV/T

Exergy investigation was carried out using the 2nd law of efficiency. It can be used to assess the system's long-term viability. It demonstrates the efficiency of heat transfer process. The investigation examined energy quality in order to determine the most efficient energy use. With a rise in T, the system was deemed to be in quasi-steady-state condition, and the specific heat of air was held constant. The mass balance equation is written as follows:

$$\sum \dot{m}_{in} = \sum \dot{m}_{out} \tag{6}$$

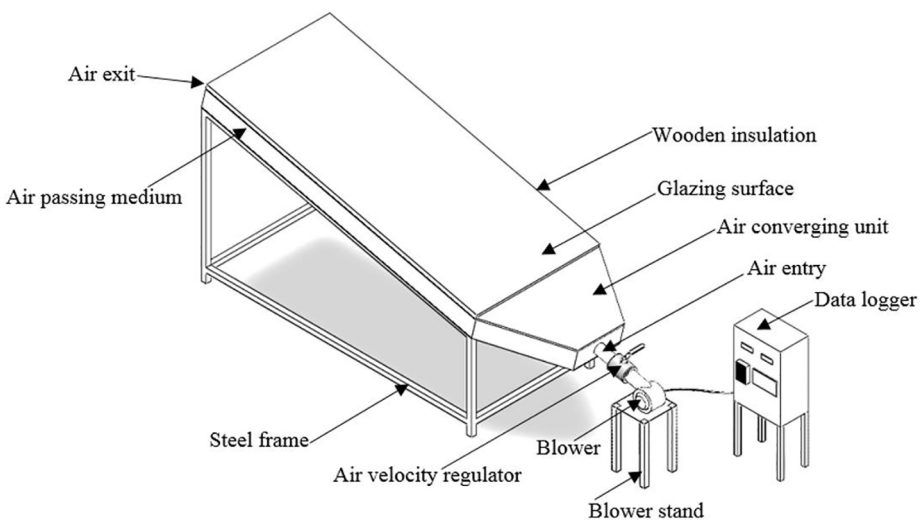

Fig. 1a. Experimental layout of PV/T system.

Fig. 1b. Photographic view of PV/T system.

Table 1
Specification of PV/T system.

Maximum Power	150 W
Weight	18 kg
Dimension	1490 * 660 * 100 mm
Open circuit voltage of solar panel, Voc	21.50 V
Short circuit current of solar panel, ISC	9.42 A
Load Voltage, V_L	17.50 V
Load current, A_L	8.57 A
Number of Cells	36
Slope of the solar panel surface	13
Overall loss coefficient, UL	5 W/m^2 K
Transmittance of the glass cover, τ	0.95
Absorptance of the glass cover, α	0.85
Collector breadth, B	658 mm
Collector breadth, H	840 mm
Area of the panel, A	98042 mm^2
Air duct length, I	1470 mm
Air duct breadth, b	645 mm
Air duct width, w	80 mm
Cross section of air entry, l × b	149 * 80 mm

Table 2
Details of forced air cooling enhancements.

SI. No	Name of cooling enhancements	Geometry	Type of air flow
1	Free duct	No fin and baffle	Straight
2	Duct with fully transverse fins	9 fins	Zigzag
3	Duct with Partially transverse fins	22 fins	Wavy
4	Duct with longitudinal fins with straight baffles	3 fins and 13 baffles	Zigzag with wavy
5	Duct with longitudinal fins with inclined baffles	4 fins and 20 baffles	Zigzag with wavy

Table 3
Air properties.

Parameters	Value
Density	1.225 Kg/m^3
Viscosity	1006.43 J/kg-k
Specific heat	0.0242 W/m-k
Thermal Conductivity	1.9 e$^{-0.5}$ Kg/m-s

Where "ṁ" = mass flow rate, and the subscript "in" stands for inlet and "out" for an outlet. The influences of kinetic and potential energy variations were disregarded; the overall energy and exergy balances can be enunciated in rate form [15].

$$\sum \dot{E}_{in} = \sum \dot{E}_{out} \tag{7}$$

$$\sum \dot{E}x_{in} - \sum \dot{E}x_{out} = \sum \dot{E}x_{irreves} \tag{8}$$

Using the Eq. (8), the rate form of the general exergy balance can be enunciated as:

$$\sum \left(1 - \frac{T_{air}}{T_s}\right) \dot{Q}_s - \dot{W} + \sum \dot{m}_{in}\,\psi_{in} - \sum \dot{m}_{out}\,\psi_{out} = \dot{E}x_{irreves} \tag{9}$$

Where

$$\psi_{in} = (h_{in} - h_a) - T_a(S_{in} - S_a) \tag{10}$$

$$\psi_{out} = (h_{out} - h_a) - T_a(S_{out} - S_a) \tag{11}$$

$$\left(1 - \frac{T_a}{T_s}\right) \dot{Q}_s - \dot{m}[(h_{out} - h_{in}) - T_a(S_{out} - S_{in})] = \dot{E}x_{irreves} \tag{12}$$

Where "Q_{solar}" is the solar energy absorbed via the panel absorber surface

$$Qsolar = G(\tau\alpha)A_{\,mod} \tag{13}$$

The exergy devastation or the irreversibility is articulated as:

$$\dot{E}x_{iireves} = T_a \dot{S}_{generate} \tag{14}$$

$$\dot{S}_{generate} = \dot{m}C_p ln\frac{T_{out}}{T_{in}} - \frac{\dot{Q}_s}{T_s} + \frac{Q_{0ut}}{T_a} \tag{15}$$

$$Q_{0ut} = \dot{Q}_s - \dot{m}C_p(T_{out} - T_{in}) \tag{16}$$

$$\eta_{exergy} = 1 - \frac{T_a\ \dot{S}_{generate}}{[1 - (T_a/T_s)]\,\dot{Q}_s} \tag{17}$$

Exergy effectiveness of a system is premeditated in relations of the net output exergy of the system or exergy devastations in the system.

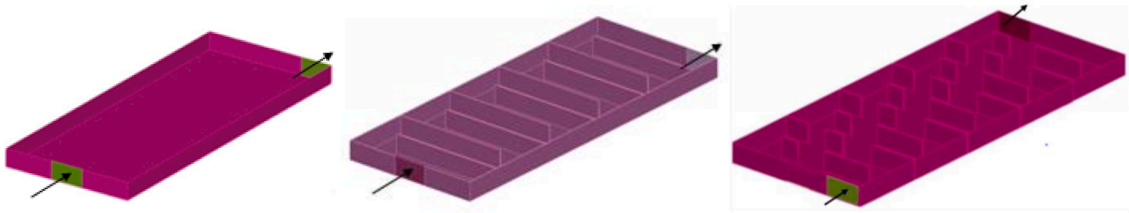

(a) Duct without fins (b) Duct with fully transverse type fins (c) Duct with partially transverse type fins

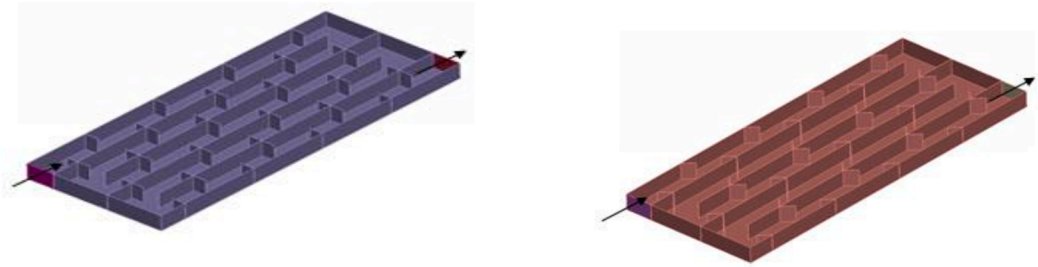

(d) Duct with longitudinal fins and straight baffles (e) Duct with longitudinal fins and inclined baffles

Fig. 2. Forced air cooling enhancements tested at PV/T system.

Table 4
Operating parameters.

Equipment	Measurement
Ambient temperature, (T_a)	30 °c
Air velocity at the entry of the channel	0.2–0.9 m/s
Solar radiation	400–1100 W/m^2

Table 5
The uncertainties of measurements.

Equipment	Measurement	Uncertainty
Thermocouples	Inlet and Outlet air channel temp	+/− 1 °C
Thermocouples	Glazing and tedlar temp	+/− 1 °C
Anemometer	Air velocity	+/− 5%
Pyranometer	Solar radiation	+/− 5%
Weather Station	Wind velocity	+/− 0.5 m/s
Mercury Thermometer	Ambient temp	+/− 0.5 °C
PV short-circuit current	Current	+/− 1%
PV open-circuit voltage	Voltage	+/− 1%
Digital Manometer	Pressure	+/− 1%

The second law effectiveness is considered as:

$$\eta_{exergy} = \frac{\dot{E}x_{out}}{\dot{E}x_{in}} = \frac{\dot{m}[h_{out} - h_{in} - T_a(S_{out} - S_{in})]}{\left(1 - \frac{T_a}{T_s}\right)\dot{Q}_s} \quad (18)$$

It's crucial to distinguish between exergy losses and annihilation while dealing with the exergy of a material contribution. Exergy devastation refers to the irreversible loss of exergy within the unit boundary, whereas exergy losses refer to exergy that passes into the environment.

$$Ex_{De} = \frac{\dot{E}x_{irreves}}{\dot{Q}_c} \quad (19)$$

All physical characteristics of air were designated as per the bulk mean T:

$$\Delta T_{mean} = (T_{in} + T_{out})/2 \quad (20)$$

The entire heat transfer coefficient for the device may be estimated because the air has acquired heat inside the designated control volume. The total heat transfer coefficient is a measure of the PV/T system's total heat absorbed. These results in the Nusselt number may be calculated,

$$Nu = h.\frac{D}{k_a} \quad (21)$$

This Nusselt number will vary while Reynolds number varies with reference to the different air velocities.

$$\text{Pressuredropofthesystem}\Delta p = (f.\left(\frac{L}{D}\right)\rho U_m^2/2) \quad (22)$$

Where ρ density of air film and U_m is average velocity of air.

Reference conditions or standard rating conditions are defined as [30]:

The solar cell temperature at reference conditions, $T_{cell,ref} = 25$ °C

The solar radiation intensity at reference conditions, $Gr_{ef} = 1000$ W/m^2

Data reduction

Steady state morals of duct air T inside at different positions are measured. These values were employed to regulate performance parameter values for assumed mass flow rate of air.

Mean air and solar panel surface Ts

The mean air $T_{film} = \frac{T_{ain} + T_{aout}}{2}$ is the arithmetic mean of restrained values of air T at exit and inlet of the test segment.

The mean solar panel surface T of all thermocouples is identified from weighted average of the T.

$Tp = \frac{\sum_{i=1}^{n} T_{pin}}{n}$ Where "n" is quantity of thermocouples.

Velocity of air over duct

The velocity of air flowing over the duct is considered from the data of mass flow rate and area of flow as

$$V = \frac{\dot{m}}{\rho WH} \tag{23}$$

Equivalent hydraulic diameter

The hydraulic diameter of the rectangular segment of the duct is demarcated as

$$D_h = \frac{2(W.H)}{(W+H)} \tag{24}$$

Reynolds number

The air flow Reynolds number of duct is considered as

$$Re = \frac{\rho V D_h}{\mu} \tag{25}$$

Where μ - dynamic viscosity.

Coefficient of heat transfer

Steady state morals of the surface and air Ts in the duct at numerous positions was employed to regulate heat provided to the air "Q_u" and heat transfer coefficient "h" as:

$$Q_u = \dot{m}\, C_p (T_{ao} - T_{ai}) \tag{26}$$

$$h = \frac{Q_u}{Ap(T_p - T_f)} \tag{27}$$

Where "ṁ" is straight restrained through employing the thermal mass flow meter in addition to "Ap" is the active heat transfer area of the absorber surface.

Nusselt number

The convective heat transfer coefficient is utilized to attain Nusselt number, Nu, as

$$Nu = \frac{hD_h}{k} \tag{28}$$

Friction factor

The friction factor was evaluated transversely along test segment length as restrained values of pressure drop, (ΔP).

$$f = \frac{2(\Delta P)D_h}{4\rho LV^2}(or) f = \frac{2(\Delta P)\rho D_h}{4LG^2} \tag{29}$$

Where $G = \frac{\dot{m}}{WH}$ is the air mass velocity

Modeling and analysis using CFD

The numerical method that can be used to evaluate the flow and thermal characteristics of fluid flow in any system are referred to as CFD. It examines systems that link fluid flow and heat transfer via computer-based replication. Using a set of mathematical governing equations to define the air flow, a numerical study of the PV/T scheme was performed.

Governing equations

CFD simulations executed to predict the flow characteristics are governed by following equations [34,48-50]:

1 The continuity equation - mass conservation

$$\frac{\partial \rho}{\partial t} + \left(\frac{\partial u}{\partial x} + \frac{\partial v}{\partial y} + \frac{\partial w}{\partial z}\right) = 0 \tag{21}$$

2 Navier-Stokes equation in the explicit vector arrangement for the conservation of x-momentum, y-momentum, z-momentum.

$$\rho\left(\frac{\partial u}{\partial t} + u\frac{\partial u}{\partial x} + v\frac{\partial u}{\partial y} + w\frac{\partial u}{\partial z}\right) = -\frac{\partial p}{\partial x} + \mu\left(\frac{\partial^2 u}{\partial x^2} + \frac{\partial^2 u}{\partial y^2} + \frac{\partial^2 u}{\partial z^2}\right) \tag{22}$$

$$\rho\left(\frac{\partial v}{\partial t} + u\frac{\partial v}{\partial x} + v\frac{\partial v}{\partial y} + w\frac{\partial v}{\partial z}\right) = -\frac{\partial p}{\partial y} + \mu\left(\frac{\partial^2 v}{\partial x^2} + \frac{\partial^2 v}{\partial y^2} + \frac{\partial^2 v}{\partial z^2}\right) \tag{23}$$

$$\rho\left(\frac{\partial w}{\partial t} + u\frac{\partial w}{\partial x} + v\frac{\partial w}{\partial y} + w\frac{\partial w}{\partial z}\right) = -\frac{\partial p}{\partial z} + \mu\left(\frac{\partial^2 w}{\partial x^2} + \frac{\partial^2 w}{\partial y^2} + \frac{\partial^2 w}{\partial z^2}\right)$$

3 Heat transfer equations

$$\rho C_p\left(u\frac{\partial T}{\partial x} + v\frac{\partial T}{\partial y}\right) = k\frac{\partial 2T}{\partial y 2} \tag{24}$$

Assumptions used in the present examination were Newtonian, incompressible, 3D and transient with all heat transfer modes. The CFD solver code Fluent was utilized in the entire study.

CFD solution

The steps followed in the CFD analysis include fluid volume extraction from the geometry of PV/T system, discretization of geometry into finite volumes (termed as meshing), quality check of meshing criteria, grid independence study, specification of flow properties and proper boundary conditions, solving numerical equations and convergence check, results extraction and interpretation, validation of results with experimental data.

The constant space of the air flow area was separated into adequately minor discrete cells, the circulation of that evaluates the locations where the flow variables were premeditated and stowed. The kind of mesh utilized was hexahedral shaped and by a complete quality of 0.93 that is recognized for management of mesh in CFD solver. The discretization of computational area is achieved through a method named Octree - a spatial subdivision procedure to discrete the flow area to limited rudiments that is an object-oriented structured meshing. The mesh quality criteria maintained in the CFD models are listed in Table 6.

The mesh dimensions were enhanced by carrying a grid-independence study as proivided in Table 7. The mesh size was sophisticated till the simulation consequences were no longer exaggerated by any additional alteration of mesh dimensions. Seeing the better arrangement by experimental information, the mesh total of 2 million was designated as there was no further development in output values after this count.

Air parameters including density and viscosity, as well as boundary conditions including the implementation of mass flow rate at the inner and outer of the PV/T system, are provided as input to numerical simulations. Furthermore, the K-Epsilon turbulence model was chosen since it is a verified and established model for dealing with air turbulence. This model is proven for such kind of flow and thermal conditions by various researches. The Semi-Implicit Method for Pressure-Linked Equations was used to conduct pressure–velocity coupling of governing equations.

Table 6
Mesh quality criteria.

Parameter	Quality criteria
Cell angle	>17°
Cell expansion rate (change of cell volume with respect to neighbouring cells)	<09
Cell skewness	0.7 to 0.9
Aspect ratio	<2000 for double precision solver
Orthogonal quality	>0.70 to ensure smooth cell size change

Table 7
Grid independence assessment.

Size of elements (mm)	Number of elements	Nusselt number (Nu)	Percentage difference
0.4	1,032,321	40.23	4.98
0.38	1,187,813	42.34	1.85
0.36	1,354,678	43.14	0.48
0.34	1,726,343	43.25	0.25
0.32	1,987,654	43.32	0.16

Results and discussion

The trials were directed depends on first and second law of efficiency respectively to study the impact of air-cooling enhancements on solar system reversibility. Then, the results were validated with developed computational model.

Effect of forced cooling enhancements on exergy effectiveness

The exergy effectiveness of PV/T scheme was performed on the base of 2nd law of efficiency through considering the exergy of solar radiation. The difference of solar radiation and average ambient T from 9 to 16 h of the day of experimentation is exposed in Fig. 3. The ambient T diverse among 32 °C to 42 °C and intensity of solar radiation found to be varied from 600 – 1100 W/m^2 throughout the day of experiment.

Figure 4 shows the exergy efficiency of air-cooling enhancements and input of PV/T system. The exergy effectiveness diverse from 25 to 36% for the duct with longitudinal fins and straight baffles. The average exergetic efficiency achieved was 25%, 27%, 31%, and 34% for ducts with fully transverse fins, partially transverse fins, longitudinal fins with straight baffles, and longitudinal fins with inclined baffles respectively. However, 21% was observed while using duct without fins or baffles. The variation of efficiency depended on the irreversibility of energy conversion process of PV/T system. The exergy efficacy enlarged when the solar intensity upsurges. The exergy loss prevailed in the range of 65–80%.

This PV/T system module operated only with 20% exergy efficiency without cooling enhancements. However, the tested cooling enhancements were able to raise the efficiency in the range of 5 % to 14 %depends on their shape and arrangement pattern. The exergy destruction factor reduced in the range of 77 to 88 % as associated to 92% of the bare PV/T system while running without these enhancements. The reason for increased efficiency was its ability to absorb whole energy of sun light.

Impact of cooling enhancements on energy efficiency

The surface T of PV/T scheme was determined by both experimentation and CFD simulation. It was detected that PV/T surface T were inversely proportional to thermal efficiency. In other words, when PV/T surface T increased, system thermal efficiency decreased. Obviously, the PV/T surface T of free duct without fins attained the highest surface T as compared to other cooling enhancements due to the absence of heat absorbing surfaces. Moreover, the horizontal straight movement of air was not able to extract heat energy from the tedlar surface.

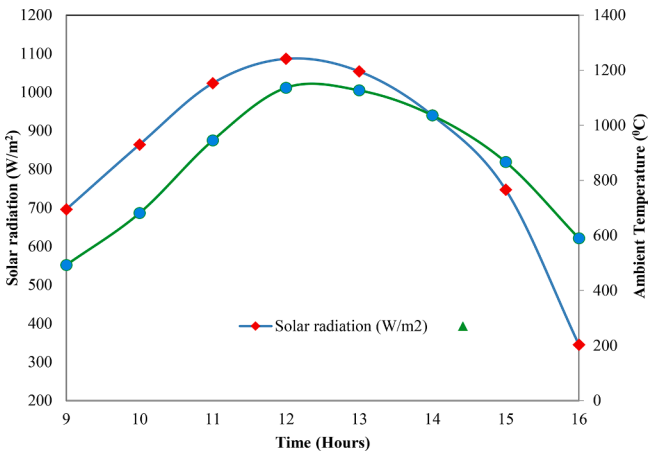

Fig. 3. Intensity of Solar radiation (W/m^2) vs. Ambient Temperature (^{0}C).

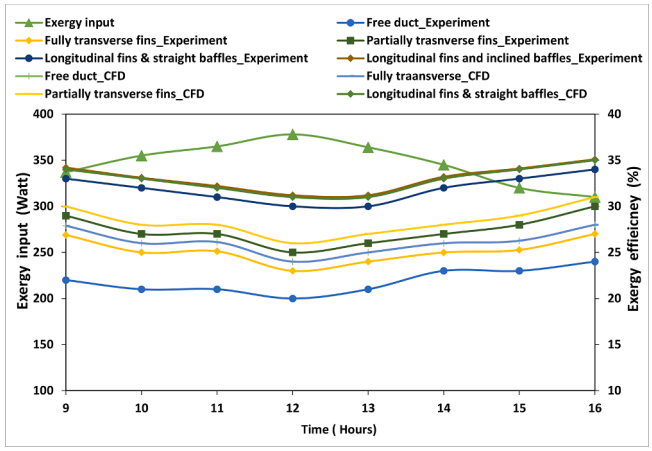

Fig. 4. Exergy efficiency for different air-cooling enhancements tested at PV/T system.

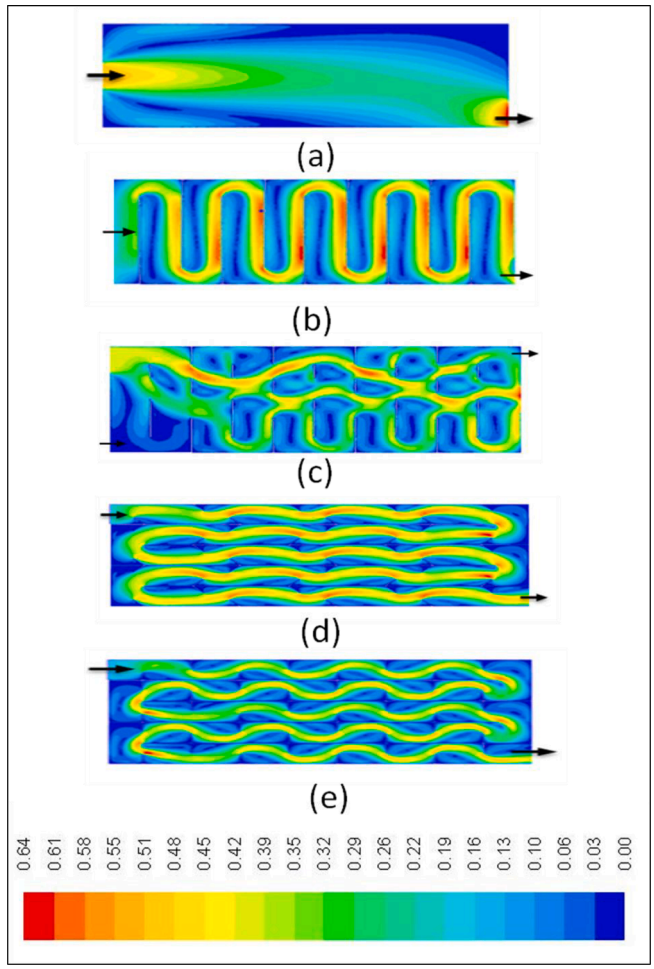

Fig. 5. Air movements of different cooling enhancements of the PV/T system.

The air velocity movements inside the ducts with different forced cooling enhancements are displayed in the Fig. 5. As shown Fig. 5(a), the fully transverse type fins in the duct created the zigzag movement of air. In the case of duct with 22 partially transverse fins (Fig. 5(b)), the wavy motions of air considerably reduced the heat. The three longitudinal fins with thirteen straight baffles induced a smooth, zigzag with wavy air movement as displayed in Fig. 5(c). This enabled the air to excerpt extra heat from the rear cross of the tedlar that effects the thermal recital of the system. The air flows through a zigzag pattern with wavy motion (Fig. 5(d)) in case of duct with four longitudinal fins with twenty inclined baffles. Due to this, contact time and area between air and tedlar surface was higher than that of other cooling enhancements. As a result, more heat transfer occurred to realize the less surface T.

The ratio between individual and overall velocity, U/U_o is plotted in Fig. 6 for all five configurations used in this study. This ratio varied from 0.35 to 0.76 for partially transverse fins whereas it varied from 0.35 to 0.75 for fully transverse fins. Longitudinal fins with straight and inclined baffles achieved the better air velocity ratio in the range of 0.35 to 0.85 because of their geometry and orientation.

Figure 7 displays the PV/T surface T measured for diverse cooling enhancements and Fig. 8 displays the exit air T. The surface T was 65° C in the free duct without fins. But it decreased to 62 °C, 61° C, 58° C, 56° C in the ducts with fully transverse fins, partially transverse fins, and longitudinal fins with straight baffles, longitudinal fins with inclined baffles respectively. The outlet air T measured was in the range 40 °C – 70 °C. The values obtained in experiments and CFD analysis showed reasonable agreement. Air T profiles of different cooling enhancements of the PV/T scheme are revealed in the Fig. 9. It is clearly visible that longitudinal fins with inclined baffles allow the air to carry more heat from the system. Therefore, more red hot spots with higher T prevailed at the duct outlet.

As revealed in the Fig. 10, the thermal energy effectiveness determined was in the range of between 12 and 18 % for the ducts with different shape and pattern of flow obstructions. The average energy efficiency achieved was 12%, 14%, 16%, and 18% for ducts with fully transverse fins, partially transverse fins, longitudinal fins with straight baffles, and longitudinal fins with inclined baffles respectively. However, only 8% thermal efficiency was observed while using duct without fins or baffles. Perhaps, it was learnt that physical geometry (shape, size, dimensions, and layout) of the obstacles influenced better thermal efficiency.

Effect of cooling enhancements on Nusselt number

The Nusselt number is additional constraint determined for the convective heat transfer mechanism of PV/T system. Its difference along the active walls were conspired in Fig. 11 as a function of Reynolds number. In all five forced convection cooling enhancements, Nu increased with Re number. The transfer degree of the heat from the lively walls to the fluid upsurges at sophisticated mass flow rates. The Nusselt number at the PV collector started with higher value at a point near to the bottom and indicate the presence of sufficient augmentation of heat transfer rate. It diminutions monotonically to a minor value at the top. Local Nusselt number was greater near the channel entry that has very small boundary layer thickness. In addition, T gradient among surface and inside air T was also very minor. Whenever boundary layer width increased, T gradient increased. This resulted in the decrease of local Nusselt number.

The Nusselt number reached was 85 in the case of the fully traverse fins. It increased to 95 while using partially traverse fins as shown in the Fig. 11(c). As shown in the Fig. 11(d), in the case of longitudinal fins and straight baffles, it increased to 120 due to relative higher heat transferring capacity than partial and full longitudinal fins. However, the longitudinal fins with inclined baffles demonstrated improved heat transfer rate because it offered wavy motion to air that enabled it to carry more heat from PV/T scheme as revealed in the Fig. 11(e).

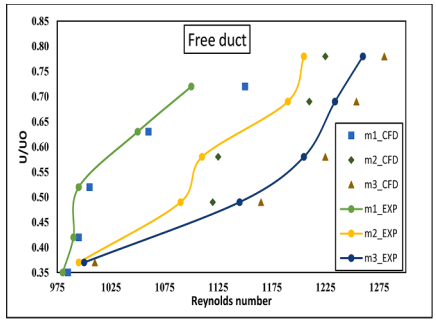

(a)

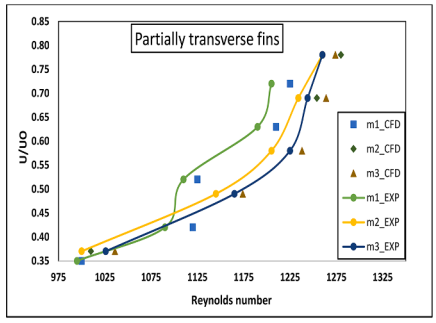

(b)

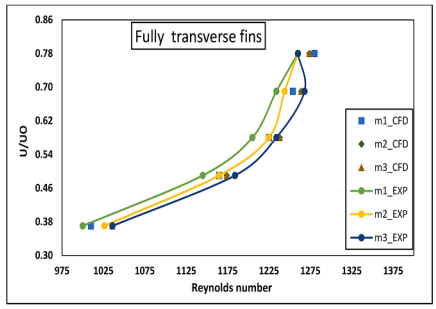

(c)

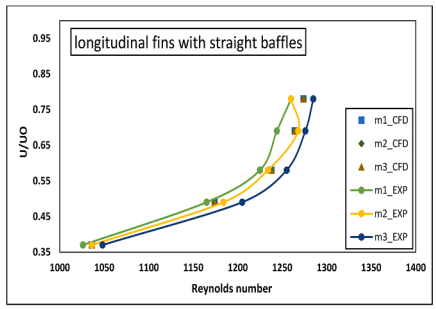

(d)

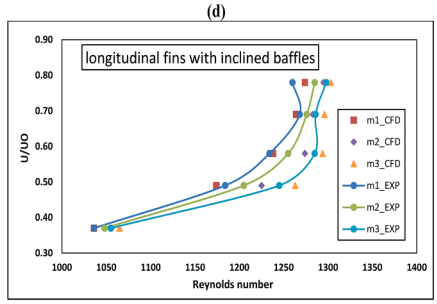

(e)

Fig. 6. U/U_o of different cooling enhancements of the PV/T scheme.

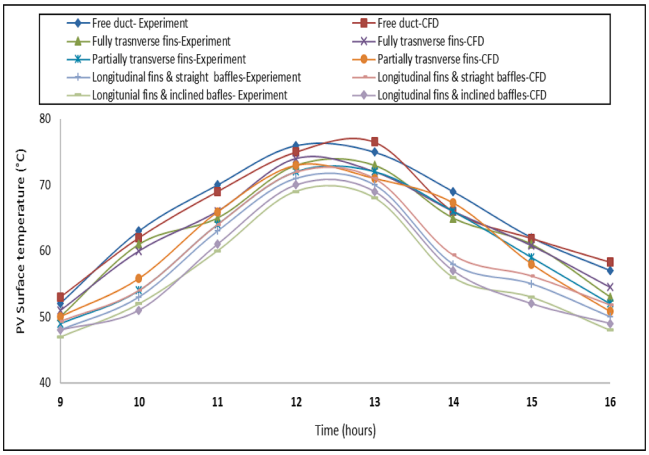

Fig. 7. PV/T Surface T for different cooling enhancements of the PV/T scheme.

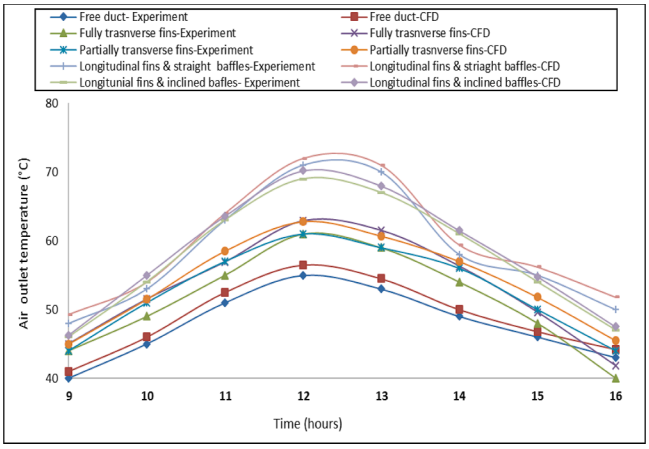

Fig. 8. Outlet air T of different cooling enhancements of the PV/T scheme.

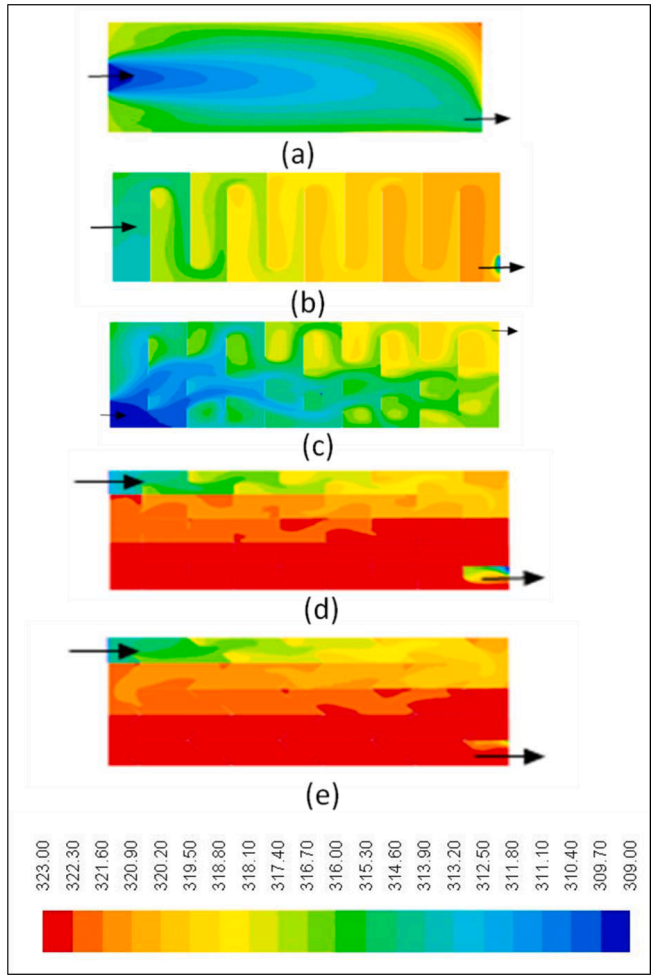

Fig. 9. Air T profiles of different cooling enhancements of the PV/T scheme.

Effect of cooling enhancements on friction factor

As the friction factor also one of the parameters that influences the heat transfer mechanism of PV/T scheme. A friction factor was determined based on the pressure drop occurred for individual cooling enhancements and plotted as shown in the Fig. 12.

Since the heat and momentum flow are related, a relationship that relate the frictional resistance to the heat transfer was obtained by Reynolds-Colburn [47]. This analogy can be written as,

$$\text{Friction factor} = 0.332Re^{-0.5}\ [40]$$

It can be observed that using the fins and baffles increase the friction factor considerably above the free duct. The longitudinal fins with inclined baffles increased the friction factor by 35%. This is the highest value as compared to other cooling enhancements. In the case of longitudinal fins with straight baffles, it increased by 20% and other fin arrangements recorded a maximum increase of 10%.

Conclusion

An energy and exergy efficiency study was executed for different air cooling enhancements of 150 W solar PV thermal collectors. The tested cooling enhancements demonstrated an improved heat removal rate from the PV/T scheme that upsurges the exergy and energy efficacy. Depends on the observation from this research, subsequent conclusions were made:

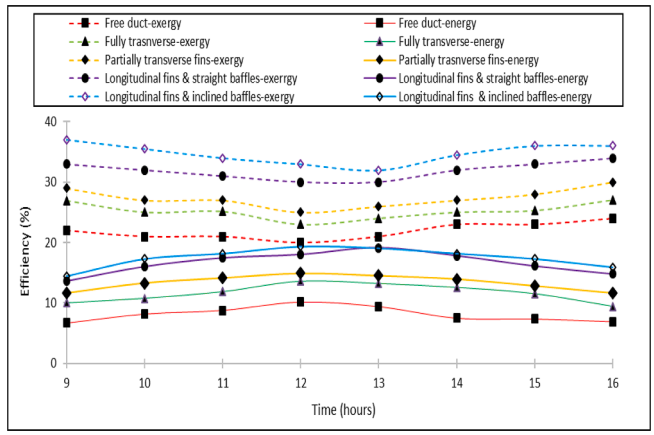

Fig. 10. Exergy and energy efficiency of different air cooling enhancements of the PV/T system.

- The exergy performance was increased from 20% to 28 % while using air cooling duct with longitudinal fins and inclined baffles. This is the maximum exergy efficiency achieved in this PV/T system
- The thermal energy performance was increased from 12 to 18 % while using air cooling duct with longitudinal fins and inclined baffles. This is the maximum energy efficiency achieved in this PV/T system with the Nusselt number ranging from 30 to 130 and Reynolds number 900–1300.

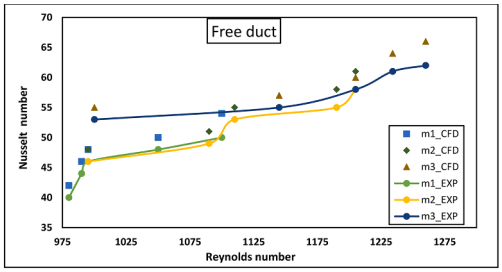

(a)

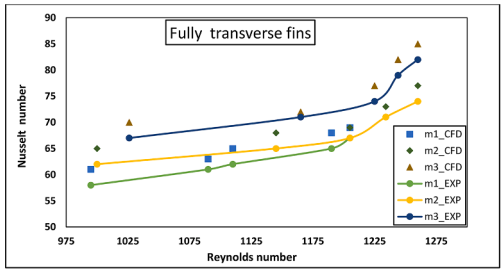

(b)

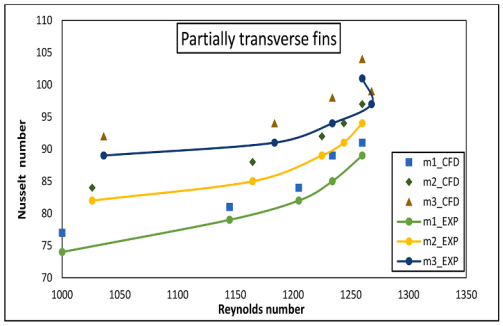

(c)

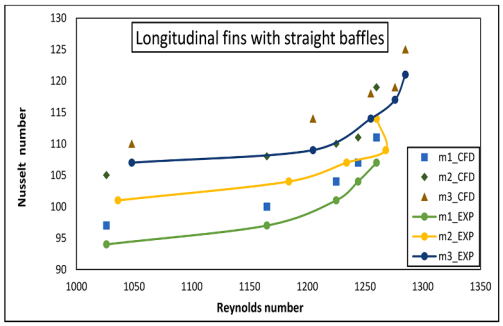

(d)

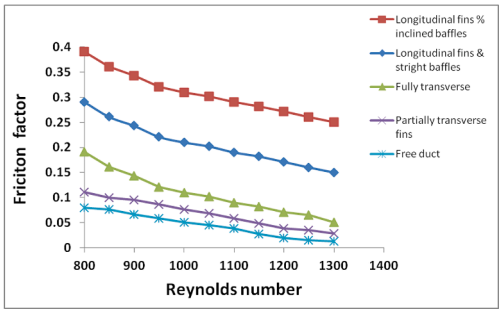

Fig. 11. Nusselt number of forced air-cooling enhancements.

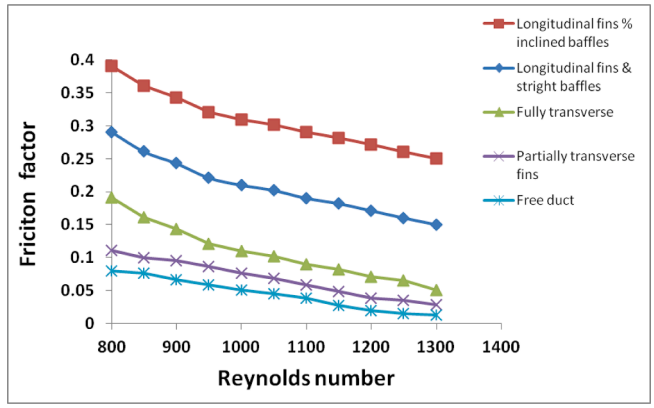

Fig. 12. Friction factor of forced air cooling enhancements.

- This study showed that Nusselt number of PV/T system upsurges with growing Reynolds number of air flow. The PV module thermal efficacy upsurges by means of growing flow rate as the friction factor increases. The longitudinal fins with inclined baffles provided higher friction factor, thereby ensured higher heat transfer rate.
- The developed Computational fluid dynamics model is identified as have virtuous contract with test consequences and can be effective in future parametric studies. Future work can be extended to focus on more optimized design of shape and arrangement of fins with baffles to get increased cooling effects, thereby efficiency.
- The fins and baffles employed in our research are economical and relaxed to manufacture and install. They bid a fairly lower friction lack in movement of air and henceforth do not necessitate higher fan power.
- On the other hands, based on the CFD model, the shape and fin arrangement can be optimized for the air cooling duct with longitudinal fins and inclined baffles
- This set up can be used for green and smart cities as it helped to reduce the energy consumption considerably.

In fact, the solar-to-power method suffers from 3 main technical flaws. The low conversion performance of solar-power is the first and most significant disadvantage. The second challenge is that solar energy harvesting demands a huge amount of land to be viable. The interruption during the night and on overcast days is the third difficulty.

CRediT authorship contribution statement

Anurag Shrivastava: Conceptualization, Data curation, Writing – original draft. **J. Prakash Arul Jose:** Conceptualization, Validation, Data curation, Writing – original draft. **Yogini Dilip Borole:** Methodology, Validation, Writing – original draft. **R. Saravanakumar:** Methodology, Validation. **Mohsen Sharifpur:** Supervision, Validation, Writing – review & editing. **Hossein Harasi:** Conceptualization, Writing – review & editing. **R.K. Abdul Razak:** Methodology, Writing – review & editing. **Asif Afzal:** Methodology, Writing – review & editing.

Declaration of Competing Interest

The authors declare that they have no known competing financial interests or personal relationships that could have appeared to influence the work reported in this paper.

References

[1] Guarracino I, Mellor A, Ekins-Daukes NJ, Markides CN. Dynamic coupled thermal-and-electrical modelling of sheet-and-tube hybrid photovoltaic/thermal (PV/T) collectors. Appl Therm Eng 2016.

[2] Singh S, Agrawal S, Avasthi DV. Design, modeling and performance analysis of dual channel semitransparent photovoltaic thermal hybrid module in the cold environment. Energy Convers Manage 2016;114:241–50.
[3] Bombarda P, Di Marcoberardino G, Lucchini A, Leva S, Manzolini G, Molinaroli L, et al. Thermal and electric performances of roll-bond flat plate applied to conventional PV modules for heat recovery. Appl Therm Eng 2016;105:304–13.
[4] Hedayatizadeh M, Sarhaddi F, Safavinejad A, Ranjbar F, Chaji H. Exergy loss-based efficiency optimization of a double-pass/glazed v-corrugated plate solar air heater. Energy 2016;94:799–810.
[5] Bahrehmand D, Ameri M. Energy and exergy analysis of different solar air collector systems with natural convection. Renewable Energy 2015;74:357–68.
[6] Yadav S, Kaushal M, Varun, Siddhartha. Exergetic performance evaluation of solar air heater having arc shape oriented protrusions as roughness element. Sol Energy 2014;105:181–9.
[7] Singh S, Chander S, Saini JS. Exergy based analysis of solar air heater having discrete V-down rib roughness on absorber plate. Energy 2012;37(1):749–58.
[8] Ozgen F, Esen M, Esen H. Experimental investigation of the thermal performance of a double-flow solar air heater having aluminium cans. Renewable Energy 2009;34 (11):2391–8.
[9] Lalji MK, Sarviya RM, Bhagoria JL. Exergy evaluation of packed bed solar air heater. Renew Sustain Energy Rev 2012;16(8):6262–7.
[10] Agrawal S, Tiwari GN. Exergoeconomic analysis of glazed hybrid photovoltaic thermal module air collector. Sol Energy 2012;86(9):2826–38.
[11] Teo HG, Lee PS, Hawlader MNA. An active cooling system for photovoltaic modules. Appl Energy 2012;90(1):309–15.
[12] Bambrook SM, Sproul AB. Maximising the energy output of a PV/T air system. Sol Energy 2012;86(6):1857–71.
[13] Alta D, Bilgili E, Ertekin C, Yaldiz O. Experimental investigation of three different solar air heaters: Energy and exergy analyses. Appl Energy 2010;87(10):2953–73.
[14] Esen H. Experimental energy and exergy analysis of a double-flow solar air heater having different obstacles on absorber plates. Build Environ 2008;43(6):1046–54.
[15] Akpinar EK, Koçyiğit F. Energy and exergy analysis of a new flat-plate solar air heater having different obstacles on absorber plates. Appl Energy 2010;87(11): 3438–50.
[16] Moummi N, Youcef-Ali S, Moummi A, Desmons JY. Energy analysis of a solar air collector with rows of fins. Renewable Energy 2004;29(13):2053–64.
[17] Chen H, Ji J, Wang Y, Sun W, Pei G, Yu Z. Thermal analysis of a high concentration photovoltaic/thermal system. Sol Energy 2014;107:372–9.
[18] Missirlis D, Martinopoulos G, Tsilingiridis G, Yakinthos K, Kyriakis N. Investigation of the heat transfer behaviour of a polymer solar collector for different manifold configurations. Renewable Energy 2014;68:715–23.
[19] Agrawal S, Tiwari GN. Overall energy, exergy and carbon credit analysis by different type of hybrid photovoltaic thermal air collectors. Energy Convers Manage 2013;65:628–36.
[20] Sabzpooshani M, Mohammadi K, Khorasanizadeh H. Exergetic performance evaluation of a single pass baffled solar air heater. Energy 2014;64:697–706.
[21] Mohammadi K, Sabzpooshani M. Appraising the performance of a baffled solar air heater with external recycle. Energy Convers Manage 2014;88:239–50.
[22] Fudholi A, Sopian K, Ruslan MH, Othman MY. Performance and cost-benefit analysis of double-pass solar collector with and without fins. Energy Convers Manage 2013;76:8–19.
[23] Hedayatizadeh M, Sarhaddi F, Safavinejad A, Ranjbar F, Chaji H. Exergy loss-based efficiency optima zation of a double-pass/glazed v-corrugated plate solar air heater. Energy 2016;94:799–810.
[24] Edgar R, Cochard S, Stachurski Z. A computational fluid dynamic study of PV cell Ts in novel platform and standard arrangements. Sol Energy 2017;144:203–14.
[25] M. Smyth, A. Pugsley, G. Hanna, A. Zacharopoulos, J. Mondol, A. Besheer, A. Savvides., 2018. Experimental performance characterisation of a Hybrid Photovoltaic/Solar Thermal Façade module compared to a flat Integrated Collector Storage Solar Water Heater module. 10.1016/j.renene.2018.04.017.
[26] Sourav Khanna, K.S. Reddy, Tapas K. Mallick. Optimization of solar photovoltaic system integrated with phase change material. Solar Energy 2018; 163: 591–599.
[27] Zolfagharnasab MH, Aghanajafi C, Kavian S, Heydarian N, Ahmadi MH. Novel analysis of second law and irreversibility for a solar power plant using heliostat field and molten salt. Energy Sci Eng 2020;8(11):4136–53.
[28] Grosu L, Mathieu A, Rochelle P, Feidt M, Ahmadi MH, Sadeghzadeh M. Steady state operation exergy-based optimization for solar thermal collectors. Environ Prog Sustainable Energy 2020;39(3). https://doi.org/10.1002/ep.v39.310.1002/ep.13359.
[29] Mandi B, Menni Y, Maouedj R, Lorenzini G, Ahmadi MH, Emani S. Improvement and nocturnal extension of the efficiency of a solar still. Int J Photoenergy 2021: 6631121.
[30] Menni Y, Ghazvini M, Ameur H, Kim M, Ahmadi MA, Sharifpur M. Combination of baffling technique and high-thermal conductivity fluids to enhance the overall performances of solar channels. Eng Comput 2020:1–22. https://doi.org/10.1007/s00366-020-01165-x.
[31] Aramesh M, Pourfayaz F, Haghir M, Kasaeian A, Ahmadi MH. Investigating the effect of using nanofluids on the performance of a double-effect absorption refrigeration cycle combined with a solar collector. Proc Inst Mech Eng Part A: J Power Energy 2019;234(981–993):981–93. https://doi.org/10.1177/0957650919889811.
[32] Jilte R, Ahmadi MH, Kalamkar V, Kumar R. Solar flux distribution study in heat pipe cavity receiver integrated with biomass gasifier. Int J Energy Res 2020;44(9): 7698–712. https://doi.org/10.1002/er.v44.910.1002/er.5502.
[33] Menni Y, Chamkha AJ, Ameur H, Ahmadi MH. Hydrodynamic behavior in solar oil heat exchanger ducts fitted with staggered baffles and fins. J Appl Comput Mech 2021. https://doi.org/10.22055/JACM.2020.32468.2021.
[34] Menni Y, Ghazvini M, Ameur H, Ahmadi MH, Sharifpur M, Sadeghzadeh M. Numerical calculations of the thermal-aerodynamic characteristics in a solar duct with multiple V-baffles. Eng Appl Comput Fluid Mech 2020;14(1):1173–97.
[35] Sadeghzadeh M, Ahmadi MH, Kahani M, Sakhaeinia H, Chaji H, Chen L. Smart modeling by using artificial intelligent techniques on thermal performance of flat-plate solar collector using nanofluid. Energy Sci Eng 2019;7(5):1649–58.
[36] Pourkiaei SM, Ahmadi MH, Ghazvini M, Moosavi S, Pourfayaz F, Kumar R, et al. Status of direct and indirect solar desalination methods: comprehensive review. Eur Phys J Plus 2021;136(5). https://doi.org/10.1140/epjp/s13360-021-01560-3.
[37] Maleki A, El Haj Assad M, Nazari MA, Rosen MA, Bui DT, Chen LG. A review of nanomaterial incorporated phase change materials for solar thermal energy storage. Solar Energy DOI: 10.1016/j.solener.2021.08.051.
[38] Mahulikar SP, Herwig H. Fluid friction in incompressible laminar convection: Reynolds' analogy revisited for variable fluid properties. Eur Phys J B 2008;62(1): 77–86.
[39] Zhang X, Tang Y, Zhang F, Lee C. A Novel aluminum-graphite dual-ion battery. Adv Energy Mater 2016;6(11):1502588. https://doi.org/10.1002/aenm.201502588.
[40] Tong X, Zhang F, Ji B, Sheng M, Tang Y. Carbon-coated porous aluminum foil anode for high-rate, long-term cycling stability, and high energy density dual-ion batteries. Adv Mater (Weinheim) 2016;28(45):9979–85. https://doi.org/10.1002/adma.201603735.
[41] Ji B, Zhang F, Song X, Tang Y. A novel potassium-ion-based dual-ion battery. Adv Mater (Weinheim) 2017;29(19):1700519. https://doi.org/10.1002/adma.201700519.
[42] Wang M, Jiang C, Zhang S, Song X, Tang Y, Cheng H-M. Reversible calcium alloying enables a practical room-temperature rechargeable calcium-ion battery with a high discharge voltage. Nat Chem 2018;10(6):667–72. https://doi.org/10.1038/s41557-018-0045-4.
[43] Mu S, Liu Q, Kidkhunthod P, Zhou X, Wang W, Tang Y. Molecular grafting towards high-fraction active nanodots implanted in N-doped carbon for sodium dual-ion batteries. Natl Sci Rev 2020;8(7). https://doi.org/10.1093/nsr/nwaa178.
[44] Kumar R, Nadda R, Kumar S, Kumar K, Afzal A, Abdul Razak RK, et al. Heat transfer and friction factor correlations for an impinging air jets solar thermal collector with arc ribs on an absorber plate. Sustainable Energy Technol Assess 2021;47:101523. https://doi.org/10.1016/j.seta.2021.101523.
[45] Santhosh Kumar PC, Naveenkumar R, Sharifpur M, Issakhov A, Ravichandran M, Mohanavel V, et al. Experimental investigations to improve the electrical efficiency of photovoltaic modules using different convection mode. Sustainable Energy Technol Assess 2021;48:101582. https://doi.org/10.1016/j.seta.2021.101582.
[46] Kumar R, Gaurav, Kumar S, Afzal A, Muthu Manokar A, Sharifpur M, et al. Experimental investigation of impact of the energy storage medium on the thermal performance of double pass solar air heater. Sustainable Energy Technol Assess 2021;48:101673. https://doi.org/10.1016/j.seta.2021.101673.
[47] Geankoplis, C.J. Transport processes and separation process principles (2003), Fourth Edition, p. 475.
[48] Mokashi I, Afzal A, Khan SA, Abdullah NA, Bin Azami MH, Jilte RD, et al. Nusselt number analysis from a battery pack cooled by different fluids and multiple back-propagation modelling using feed-forward networks. Int J Therm Sci 2021;161: 106738. https://doi.org/10.1016/j.ijthermalsci.2020.106738.
[49] Afzal A, Mokashi I, Khan SA, Abdullah NA, Azami MHB. Optimization and analysis of maximum temperature in a battery pack affected by low to high Prandtl number coolants using response surface methodology and particle swarm optimization algorithm. Numer Heat Transf Part A Appl 2021;79(5):406–35. https://doi.org/10.1080/10407782.2020.1845560.
[50] Afzal A, Samee ADM, Jilte RD, Islam T, Manokar AM, Abdul K. Battery thermal management : An optimization study of parallelized conjugate numerical analysis using Cuckoo search and Artificial bee colony algorithm. Int J Heat Mass Transf 2021;166:120798. https://doi.org/10.1016/j.ijheatmasstransfer.2020.120798.